Nanoscale

PAPER

View Article Online
View Journal | View Issue

Cite this: *Nanoscale*, 2025, **17**, 12503

In chemico categorization of magnetite-, hydroxyapatite-, and Ag-derived hybrid nanobiomaterials based on the surface oxidative reactivity: implications of doping and coating†

V. Alcolea-Rodriguez, *‡[a] I. Fenoglio, [c] M. Blosi, [b] M. Serantoni, [b] F. C. Simeone, [b] I. Zanoni, [b] A. L. Costa,[b] R. Portela [a] and M. A. Bañares *[a]

In chemico tests are important tools that complement *in silico*, *in vitro* and *in vivo* approaches to predict the toxicological impact of nanomaterials (NMs). Here, we apply a recently proposed *in chemico* methodology, based on the evaluation of the number, nature and properties of reactive surface sites of NMs, to a series of magnetite-, hydroxyapatite- and silver-based hybrid nanobiomaterials (NBMs). The properties of the NBMs were examined using methanol chemisorption followed by temperature-programmed surface reaction (MeOH-TPSR), dithiothreitol (DTT) oxidation, cyclic voltammetry in biologically relevant media, and electron paramagnetic resonance (EPR) spectroscopy in a series of relevant media as a spin trap. The resulting data were critically compared and correlated with the available *in vitro* data of the NBMs' hazard. Our findings reveal significant differences in the oxidative potential of these hybrid NBMs. Iron (Fe) doping in hydroxyapatite (HA) introduced new redox-active surface sites, leading to increased oxidative reactivity *via* ROS-independent mechanisms, as evidenced by higher DTT depletion and Fenton-like activity compared to HA. Conversely, titanium (Ti) doping modified HA's surface by introducing acidic active sites, reducing its oxidative capacity. Coating Fe_3O_4 with poly(ethylene glycol)-poly(lactic-*co*-glycolic) acid (PEG-PLGA) enhanced the oxidative reactivity without ROS generation, suggesting a surface-driven process. In contrast, hydroxyethyl cellulose (HEC) coating significantly reduced the high reactivity of uncoated silver (Ag). This study underscores the importance of determining the NBMs' reactivity profile for safe biomedical use, highlighting how specific coatings and dopants can transform oxidative surface properties.

Received 17th February 2025,
Accepted 12th April 2025

DOI: 10.1039/d5nr00709g

rsc.li/nanoscale

Introduction

The integration of nanotechnology and biotechnology has enabled the development of advanced hybrid nanobiomaterials (NBMs) for applications in medical devices, diagnostics, and tissue regeneration.[1] To address clinical challenges like pathogen adhesion and biofilm formation, coatings or doping strategies are proposed to modify the surfaces of common NBMs,[2] such as magnetite,[3,4] hydroxyapatite (HA),[5,6] and silver[7,8] nanoparticles, altering the number and nature of their surface sites, which in turn changes their oxidative reactivity.[9,10] This reactivity can be a double-edged sword; it may induce toxic effects,[11] but it can also serve as an antimicrobial agent[12] with potential applications in areas like food packaging[13] or a redox regulator in neurodegenerative diseases.[14]

Toxicity testing for NBMs, often referred to as nanosafety, is complicated by the growing diversity of their property variants. Nanosafety assessment has traditionally relied on *in vivo* tests, which are not only time-consuming and resource-intensive, but also increasingly misaligned with global efforts to reduce animal testing.[15,16] Therefore, new approach methodologies (NAMs), based on *in silico*,[17,18] *in chemico*[19,20] and *in vitro*[11,21–25] approaches, have appeared as promising alternatives[26–28] unified by a singular objective to facilitate the prediction of the potential hazard or toxicity of nanomaterials, while simultaneously reducing animal testing and the costs of assays.[29,30] This endeavor necessitates the comprehensive

[a]*Instituto de Catalisis y Petroleoquimica ICP-CSIC, C/Marie Curie 2, 28049 Madrid, Spain. E-mail: valcolear@gmail.com, miguel.banares@csic.es*
[b]*CNR-ISSMC, National Research Council of Italy-Institute of Science, Technology and Sustainability for Ceramics, Faenza, Italy*
[c]*Dipartimento di Chimica, Università di Torino, via P. Giuria 7, 10125 Torino, Italy*
†Electronic supplementary information (ESI) available. See DOI: https://doi.org/10.1039/d5nr00709g
‡Current address: CNR-Institute for Photonics and Nanotechnologies (CNR-IFN), Milan, 20133, Italy.

characterization of various properties and the establishment of robust correlations between them.[31,32]

Assessing not only the physicochemical but also the biological identity of NBMs, *i.e.*, their characteristics and properties in physicochemical and biological media, is crucial for determining the likelihood of NBMs initiating hazardous events and how their intensity is modulated.[33,34] Though effects attributable to particle composition, size and morphology cannot be disregarded, those related to surface chemistry-dependent phenomena are predominant, particularly in metal and metal oxide nanoparticles.[19,35] A spectrum of complementary cellular and acellular techniques can be employed to derive specific descriptors, ideally correlating with *in vitro*[25,36] or *in vivo*[37–39] adverse effects, thereby helping to determine the modes of action (MoA) and thus providing extrapolating criteria for the safe-and-sustainable-by-design (SSbD) development of NBMs.[32] Additionally, these descriptors can be used for the identification and development of redox-active nanomaterials, of increasing interest for therapeutic purposes in the nanomedicine field.[40] Thus, surface charge, surface chemistry or surface defect-dependent oxidation or reduction processes[41–44] are important descriptors that should be evaluated in relevant exposure media to better correlate with biological responses, as any surrounding conditions may alter these properties.[45] Obviously, characterization techniques that quantify the number and nature of reactive surface sites and reactive oxygen species (ROS) production provide valuable descriptors for assessing the redox reactivity, which involves electron transfer during reduction and oxidation reactions,[46,47] and correlating it with oxidative stress damage in cells, one of the most accredited mechanisms driving nanomaterials' toxicity.[48–50]

The aim of this work is to analyze the surface property modifications induced by metal doping in nano-HA or by organic coatings on Ag- and Fe_3O_4-derived NBMs, as case studies representative of commonly used metal-containing NBMs. An *in chemico* multi-technique methodology is proposed for quantifying the number and nature of reactive surface sites and evaluating redox reactivity. The methodology involves gas-phase methanol chemisorption followed by temperature-programmed surface reaction (MeOH-TPSR) for reactive site quantification and categorization; liquid-phase probe reactions such as dithiothreitol (DTT) oxidation, for general oxidative potential assessment, and salicylic acid hydroxylation, for OH radical generation; spin-trap methods to identify free radicals by electron paramagnetic resonance (EPR) analysis; and cyclic voltammetry to determine surface-driven oxidation processes.

Experimental

Materials and reagents

The NBMs analyzed in this study include two lab-scale doped hydroxyapatites (FeHA and TiHA),[51] a commercial magnetite with a bioresorbable organic coating of poly(ethylene glycol) and poly(lactic-*co*-glycolic) acid from Colorobbia Italia SpA (Fe_3O_4_PEG-PLGA),[34] and lab-scale silver nanoparticles coated with a shell of hydroxyethyl cellulose (AgHEC).[52,53] These NBMs were supplied through the BIORIMA EU project materials repository and were selected based on their biomedical relevance, extensive prior characterization, and commercial availability. Hydroxyapatite, magnetite, and silver are examples of NBMs already used in biomedical applications, and functionalization strategies such as coating and doping are commonly employed to enhance their biocompatibility and efficacy. These materials are categorized as biomimetic and/or bioresorbable and are capable of eliciting specific cellular responses at the molecular level.[54,55] In addition, CuO, HA, Fe_3O_4, and Ag NP reference materials were purchased from Sigma-Aldrich for comparison. Dulbecco's Modified Eagle's Medium (DMEM) with fetal bovine serum (FBS) was prepared by mixing DMEM without sodium pyruvate with 10%v/v FBS (both from Thermo Fisher Scientific) at room temperature.

Physicochemical characterization

The physicochemical and biological characteristics of the target samples were assessed by performing analyses in a powder or liquid suspension state. For the liquid-phase experiments, the powdered nanomaterials (HA, Ag, Fe_3O_4, TiHA, and FeHA) were dispersed according to the NanoGenoTox protocol,[56] whereas the colloidal samples (Fe_3O_4_PEG-PLGA and AgHEC) were first diluted in Milli-Q water to a concentration of 256 ppm and then diluted in the selected media.

Specific surface area. All nanomaterials were pretreated by degassing for 16 h at 120 °C prior to measurement using Micromeritics ASAP 2020 nitrogen adsorption isotherm equipment. The specific surface area was calculated using the BET equation.

Hydrodynamic diameter and zeta potential. The hydrodynamic diameter (d) and polydispersity index (PDI) of the nanosuspensions in all media as well as the zeta potential (ζ) were determined by dynamic light scattering (DLS) and electrophoretic light scattering (ELS) measurements, respectively, using a Zetasizer Nano instrument ZSP (model ZEN5600, Malvern Instruments, UK). Instrument settings are detailed in the ESI,† while ζ data with the relative standard deviation (RSD, %) were obtained by averaging the signal of three measurements.

Dissolution. Static dissolution measurements were performed to assess the release of $Fe^{2+/3+}$ and Ag^{+} from the nanoparticles at established incubation time points. The experimental procedure is schematized in Fig. S1.† The dispersion was diluted in the relevant media (at concentrations of 10–50 mg L^{-1} (ppm)) and incubated in a thermal bath for 1 h and 24 h at 37 °C. The ion release rate was calculated as the ratio between the dissolved ions after ultrafiltration and the total iron (Fe-based NPs and $Fe^{2+/3+}$) or silver (Ag-based NPs and Ag^{+}) present in the initial suspension, expressed as percentage. The results from ICP-OES were reported as the average of three independent measurements with the relative standard deviation (RSD).

Surface and redox reactivity

Reactive site quantification and categorization using methanol as a probe molecule. Reactive site quantification and classification were performed by gas-phase methanol chemisorption and temperature-programmed surface reaction (TPSR) experiments as described elsewhere.[19,20] Briefly, 250–500 mg of nanomaterials (mesh size <100 μm) diluted with 500 mg of SiC was placed in a fixed-bed reactor. The sample was pretreated at 450 °C in an air flow of 150 mL min^{-1} for 35 min to remove moisture and impurities. Then, the sample was cooled down to 100 °C, purged with Ar (100 mL min^{-1}), and fed with 2000 ppm methanol in argon with 5% helium (100 mL min^{-1}). Upon saturation, the sample was purged with 100 ml min^{-1} Ar and heated to 450 °C at 10 °C min^{-1} under Ar. The reaction products were detected by mass spectrometry (see the details in the ESI†), defining the reactivity of NBMs' surface sites; dimethyl ether (DME) was desorbed for acid sites, CO_2 was desorbed for basic or highly redox (over-oxidation) and formaldehyde was desorbed for redox sites. Equivalent blank tests were performed with 500 mg SiC without the NBMs.

Dithiothreitol (DTT) consumption as a probe for oxidative potential assessment. To quantify the oxidative potential of the NBMs, dithiothreitol consumption experiments were performed as described elsewhere.[19,57] Briefly, 3 mL of 200 μg mL^{-1} NM dispersion in 1 mM phosphate buffer was incubated for 1 h at 37 °C and 500 rpm with 3 mL of 100 μM DTT water solution. Then, the nanomaterials were removed by filtration and the filtrate was mixed with an equal volume of 1 mM Ellman's reagent (5,5′-dithiobis-(2-nitrobenzoic acid)) to quantify the non-oxidized DTT at 412 nm by UV-vis spectrophotometry (calculation details are provided in the ESI†). As a negative control, the same procedure was followed without the NMs to evaluate and subtract from the results the spontaneous oxidation of DTT. 30 wt% H_2O_2 was used as a positive control to calculate the normalized index of oxidant generation (NIOG).[19,58] Additionally, CuO nanoparticles obtained from Sigma-Aldrich (ref: 544868) were used as a reference to compare the reactivity with a well-characterized engineered nanomaterial (NIOG ≈ 1).

Statistical analysis. The DTT depletion values were used to classify the reactivity of the NBMs using K-means clustering applied to the NIOG and significant differences were confirmed between the NBMs for all parameters (NIOG, OP-area and OxTOF) using *t*-tests ($p < 0.05$).

Salicylic acid as a probe for OH radical generation. Salicylic acid is an OH radical scavenger that can be used for its indirect detection if the sample does not have any other radical scavenger and all the OH radicals generated by the nanomaterial react with salicylic acid to give dihydroxybenzoic acid hydroxylation products (Fig. S2†).[59,60] Due to the low production of OH radicals, it was not possible to detect the decrease in the concentration of salicylic acid, so it was estimated from the hydroxylation reaction yield using OH radicals produced by 10 μM hydrogen peroxide subjected to UV irradiation. The production of OH radicals was evaluated in suspensions containing the nanomaterial under investigation at a concentration of 100 ppm, 10 mM phosphate buffer (pH 7.4), 50 μM salicylic acid, and 10 μM hydrogen peroxide. The suspensions were kept under magnetic stirring for 24 h, filtered, and subsequently analyzed using a HPLC system equipped with a C18 column and a fluorescence detector. The OH radical formation rate was obtained using eqn (1):

$$\nu_{OH} = \frac{\nu_{2,5\text{-DHBA}}}{f_{(2,5\text{-DHBA})}} \quad \nu_{OH} = M_{\text{salycilic acid}} \frac{\nu_{2,5\text{-DHBA}}}{M_{2,5\text{-DHBA}}} \tag{1}$$

where ν_{OH} represents the OH radicals produced in one hour per liter of solution (nM h^{-1}) and $\nu_{2,5\text{-DHBA}}$ is the 2,5-dihydroxybenzoic acid produced in one hour per liter of solution (nM h^{-1}).[61] Finally, $f_{(2,5\text{-DHBA})}$ is obtained as the ratio between the molecular weights of 2,5-DHBA and salicylic acid (eqn (2)).

$$f_{(2,5\text{-DHBA})} = \frac{M_{2,5\text{-DHBA}}}{M_{\text{salicylic acid}}} \tag{2}$$

Electronic paramagnetic resonance (EPR) monitoring of free radical species. The generation of free radical species was monitored by electron paramagnetic resonance (EPR) spectroscopy (Miniscope 100 EPR spectrometer, Magnettech, Berlin, Germany). Instrument settings: microwave power: 7 mW, modulation amplitude: 1G, scan time: 80 s, and two scans. Different probe reactions were performed to decipher free radical generation. For the production of superoxide and hydroxyl radicals, 0.5/6.8 mg of each sample were suspended in 730 μL of a buffer solution (14 mM potassium phosphate buffer pH 7.4) containing 60 mM DMPO (5,5-dimethyl-1-pyrroline-*N*-oxide, Enzo Life Sciences, Inc.) and the suspension was constantly stirred. For reactivity mediated by ROS and surface reactive sites, 1/12 mg of each sample were suspended in 2 mL of phosphate buffer containing 50 mM TEMPONE-H (1-hydroxy-2,2,6,6-tetramethyl-4-oxo-piperidine, Enzo Life Sciences, Inc.) and the suspension was constantly stirred. Finally, for the Fenton reaction, 0.5/6.8 mg of each sample were suspended in 730 μL of a buffer solution (14 mM potassium phosphate buffer pH 7.4) containing 60 mM DMPO and 27 mM H_2O_2 and the suspension was constantly stirred. The EPR spectra of all the samples and reactions were recorded in 50 μL of the suspension withdrawn after 60 min. For FeHA and Fe_3O_4_PEG-PGLA, the experiments were repeated after incubation of the samples at 37 °C for 24 h in DMEM + 10% FBS under agitation (0.5 mg ml^{-1}), followed by isolation through three centrifugation/dispersion cycles in PBS.

Simulations of the spin trapping/EPR spectroscopy experimental signals were performed by using the software Winsim2002 (version 0.98, National Institute of Environmental Health Science, National Institutes of Health, USA). The hyperfine splitting constants obtained from the simulation optimization were compared with those reported in the literature (NIESH S.T.B.D. database).

Cyclic voltammetry for the assessment of redox potential. The redox potentials of target materials were quantified from

the cyclic voltammograms obtained from a conventional 3-electrode electrochemical cell controlled with a potentiostat. The NBMs were anchored at the top of a glassy carbon electrode (GC) by pressing them toward it.[62] A modified GC was used as the working electrode and the reference electrode was a calomel electrode (SCE) with a Pt counter electrode. The redox potentials of the NMs were calculated from the reduction and oxidation peaks that appeared in the cyclic voltammogram. Reduction and oxidation peaks were recorded in an aqueous electrolyte (10^{-2} M K_2SO_4) and in DMEM.

Results

Dissolution test and colloidal behavior

The results of static dissolution tests and colloidal characterization conducted in water and in complete medium (DMEM + FBS) for different NBM concentrations are reported in the ESI (Table S1 for Fe-based NBMs and Table S2 for Ag-based NBMs†).

The three iron-based magnetic NBMs (Fe_3O_4, Fe_3O_4_PEG-PLGA and FeHA) exhibit poor solubility in complete medium with concentrations below the limit of detection (0.01 mg L^{-1}). Uncoated Fe_3O_4 showed a strong tendency to agglomerate, despite the actual particle size being <200 nm. This behavior may negatively affect its dissolution and dispersion properties, potentially limiting its bioavailability. Moreover, it exhibited size variability and a concentration-dependent behavior. In complete medium, the average particle size of Fe_3O_4 initially decreased due to agglomerate disaggregation or partial dissolution. However, after 24 h of incubation, particle coarsening occurred, likely due to the saline environment. Fe_3O_4_PEG-PLGA in water at neutral pH showed a stable hydrodynamic behavior, with a small particle size (70 nm) and a negative surface charge (ζ = −50 mV), consistent with the PEG-PLGA coating. In DMEM + FBS, however, the ζ value leveled off to −10 mV and a concentration-dependent increase in size was observed at higher concentrations (50 ppm), indicating reduced colloidal stability. FeHA exhibited a stable hydrodynamic diameter of 250–300 nm in water with a negative ζ value. In DMEM + FBS, protein adsorption improved dispersion and reduced the particle size at low concentrations (10 ppm), but after 24 h, coarsening occurred, leading to reduced colloidal stability. The ζ value also shifted to around −13 mV, which is consistent with the typical behavior in complete medium (Table S1†). Concentration-dependent iron dissolution was noticed with no release at 50 ppm, but *ca.* 5% iron release from FeHA at 10 ppm after 24 h was observed, suggesting that lower concentrations may promote slight dissolution in biological media.

Two silver-based NBMs were tested for their colloidal and dissolution behavior, Ag and AgHEC. Dissolution of Ag NPs in complete culture medium was equivalent to that of AgHEC at 50 ppm (0.2%), but more pronounced at lower concentrations (1.7% *vs.* 0.8% at 10 ppm) with a slight increase after 24 h of incubation. In water, the commercial uncoated silver exhibited larger hydrodynamic diameters than AgHEC, synthesized in liquid suspension, a typical behavior of dry nanopowders, which tend to aggregate. Despite the dispersion effect expected in DMEM + FBS, Ag particle coarsening was observed, together with a decrease in the value of ζ, probably ascribable to the higher ionic strength of the medium. In DMEM + FBS, the particle size of AgHEC decreased significantly and a negative ζ value was observed. Lower standard deviations and moderate PDI values indicated a more stable suspension compared to Ag NPs.

Number and nature of surfaces sites

The specific surface area was analyzed using N_2 adsorption isotherms for all powder nanomaterials (Fig. 1, left) but for three samples, namely Ag, due to its low porosity and, thus, low N_2 adsorption, and the coated Fe_3O_4_PEG-PLGA and AgHEC NBMs, because the polymeric coating would collapse in the dry state. TiHA presented the highest specific surface area (95 m^2 g^{-1}), followed by FeHA (77 m^2 g^{-1}), whereas HA (18 m^2 g^{-1}) and Fe_3O_4 (6 m^2 g^{-1}) had the lowest surface areas. Fe- and Ti-doped HA exhibited a high methanol chemisorption (0.23 and 0.19 mmol g^{-1}, respectively), comparable to the Fe_3O_4 reference material, with the highest value despite its low surface area. The trend is thus reversed for the active site surface density (Fig. 1, right); HA exhibits more active sites per unit of surface than the doped hydroxyapatites.

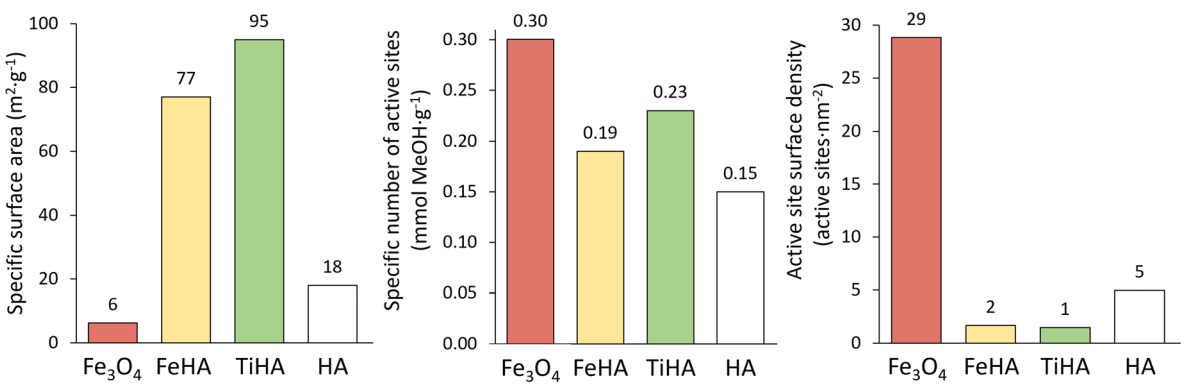

Fig. 1 Left, specific surface area obtained using the N_2 adsorption isotherm (BET). Middle, number of sites per gram. Right, active site surface density obtained by a combination of methanol chemisorption and BET data.

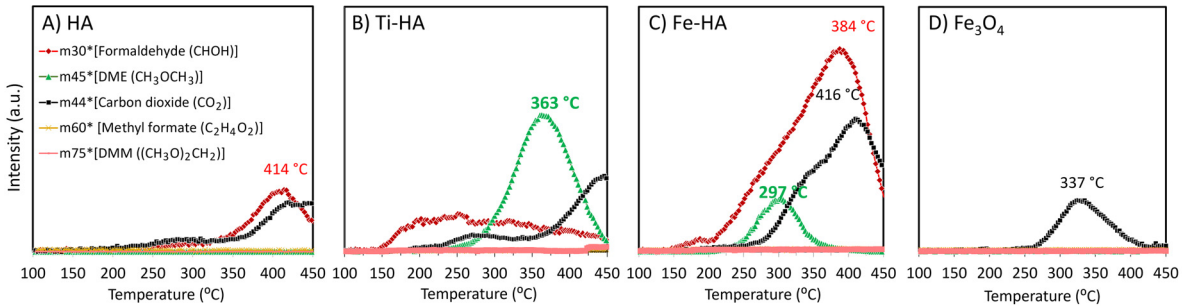

Fig. 2 Temperature-programmed surface reaction products of pre-adsorbed methanol for HA (A), TiHA (B), FeHA (C) and Fe_3O_4 (D).

MeOH-TPSR was used to assess the nature of reactive surface sites for four different nanomaterials. HA (Fig. 2A) has low, mainly redox and basic reactivity with small amounts of carbon dioxide and formaldehyde detected as reaction products. Doping modifies the picture; Ti introduces acid reactivity, not detected in undoped HA, as reflected by the dimethyl ether signal (Fig. 2B). In addition, a decrease in the amount of formaldehyde is observed. Conversely, the amounts of formaldehyde and carbon dioxide significantly increase in the Fe-doped HA (Fig. 2C), which reflects a marked enhancement of redox and basic reactive surface sites, along with some acidity, indicated by a small dimethyl ether signal. In contrast, Fe_3O_4 (Fig. 2D) showed just basic surface sites, desorbing CO_2 with a peak maximum at 337 °C. This relatively high temperature for maximum formation of carbon dioxide is closely associated with a limited reactivity of the surface sites, discarding oxidative reactions as the origin. Previous studies reported that for CuO, for example, maximum conversion to CO_2 was observed at a temperature as low as 221 °C,[19] which was attributed to methanol over-oxidation.

Oxidative potential

So far, several different pathways resulting in oxidative stress are known for nanomaterials. The most common mechanism involves redox-active NMs, which can unbalance the redox homeostasis of cells by generating ROS, degrading biomolecules by reaction with surface active sites, or consuming antioxidant molecules.[58] In this paper, we have estimated (1) the ROS generation by the salicylic acid method and by EPR spectroscopy, (2) the presence of reactive surface sites by methanol-TPSR, and (3) the ability to consume antioxidants by the DTT assay.

Thiol oxidation. Dithiothreitol (DTT) is a probe that can be used to monitor the capability of NMs to oxidize thiols.[63–65] Thiols like glutathione (GSH) or cysteine (Cys), with high-affinity binding sites of metals, such as zinc or iron, are largely involved in the protection of cells from oxidative stress.[66] Oxidation of thiols occurs through a one-electron oxidation reaction, giving sulfur-centered radicals that dimerize in disulfide:

$$\mathrm{R{-}SH} \rightarrow \mathrm{R{-}S^{\bullet}} + \mathrm{H^{+}} + \mathrm{e^{-}}$$

$$2\ \mathrm{R{-}S^{\bullet}} \rightarrow \mathrm{R{-}SS{-}R}$$

The oxidative potentials of different NBMs evaluated by the DTT assay according to different descriptors (see the ESI, section 2.3 and Table S3†) are presented in Fig. 3. K-means clustering classified the NBMs into low, moderate, and high

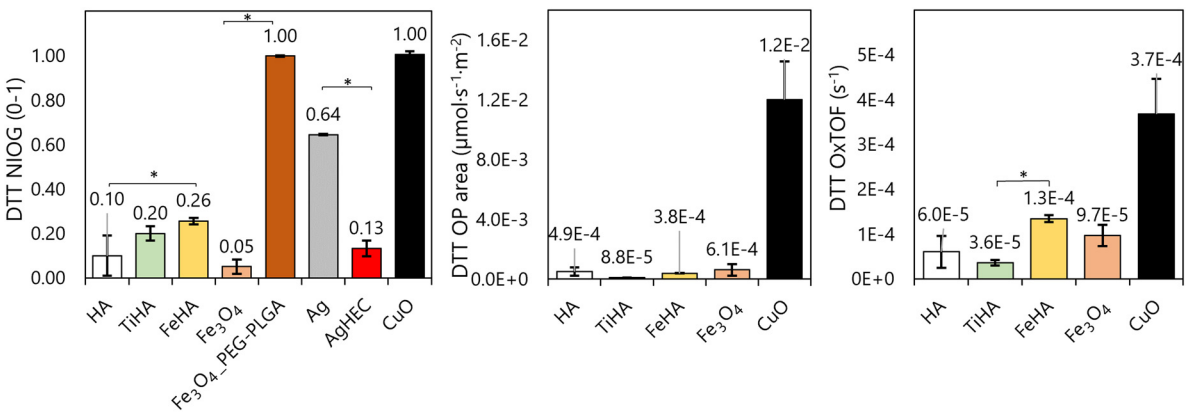

Fig. 3 Oxidative potential obtained by the DTT assay. DTT depletion normalized by a positive control, NIOG (left), DTT oxidation rate normalized per area (middle), and per reactive site, OxTOF (right). The statistical significance of pairwise comparisons was evaluated using *t*-tests (*, $p < 0.05$) between the related NBMs (FeHA/TiHA *vs.* HA, Ag *vs.* AgHEC, or Fe_3O_4 *vs.* Fe_3O_4_PEG-PLGA).

reactivity groups, while pairwise comparisons between the related NBMs (*e.g.*, FeHA/TiHA *vs.* HA, Ag *vs.* AgHEC, or Fe_3O_4 *vs.* Fe_3O_4_PEG-PLGA) were performed using *t*-tests ($p < 0.05$). Among the HA-based nanomaterials, both dopants increased the overall reactivity as measured using the NIOG parameter (0.20 for TiHA and 0.26 for FeHA). However, only FeHA showed a statistically significant difference compared to HA (NIOG ≈ 0.10). For iron-based nanomaterials, the PEG-PLGA coating of Fe_3O_4 significantly enhanced the oxidative potential as compared to the uncoated Fe_3O_4. This unexpected effect of the polymeric coating might be related to the higher exposed surface of the coated magnetite, which does not aggregate as the coated one. The trend was reversed for silver-based materials, as uncoated Ag NPs' reactivity was one of the highest in the series, whereas Ag coated with HEC presented one of the lowest oxidative potential values, justifying its use as a safe-by-design strategy for the development of Ag-based antimicrobial agents.[52,53]

DTT oxidation rates (mol DTT s^{-1}) were normalized based on two parameters: physical surface area (μmol DTT s^{-1} m^{-2}) and reactive site number (DTT OxTOF, s^{-1}) – nanomaterials for which the BET surface area could not be measured were excluded from this analysis. When normalized per surface area, the thiol oxidation rates of all tested NBMs were relatively slow compared to the CuO positive reference (Fig. 3, middle panel). When comparing the DTT OxTOF, this difference was reduced, particularly for FeHA (Fig. 3, right). Therefore, although the overall surface reactivity of the tested NBMs is low compared to CuO, the reactivity per reactive site is not negligible, with FeHA demonstrating one-third of CuO's thiol group oxidation rate. FeHA exhibited markedly higher reactivity compared to HA (and even Fe_3O_4), reflecting the influence of the dopant on the oxidative properties of hydroxyapatite-based nanomaterials.

Finally, K-means clustering analysis of DTT NIOG values classified Fe_3O_4_PEG-PLGA as a highly reactive NBM, alongside the control CuO. Ag stood out as a moderately reactive NBM, while Fe_3O_4, HA, TiHA, FeHA, and AgHEC were grouped as low-reactivity NBMs.

ROS generation. The ability to generate hydroxyl or superoxide radicals from water or dissolved oxygen was evaluated using the EPR spectroscopy/spin trapping technique and salicylic acid test. As expected for the NBMs, none of the tested samples generated ROS, as inferred from the results of both analyses, except for Fe_3O_4_PEG-PLGA that was able to oxidize salicylic acid to 2,5-dihydroxybenzoic acid in small amounts (data not shown). To further assess the possible reactivity of the NBMs, the probe molecule TEMPONE-H was used as a spin trap. This probe reacts with both ROS and surface reactive sites, generating the radical TEMPONE that is detected by EPR spectroscopy as a typical three line-signal:

$$\text{TEMPONE-H} \rightarrow \text{TEMPONE}^{\bullet} + H^{+} + e^{-}$$

It is therefore suitable to monitor a general reactivity at the surface/water interphase. In this case, Fe_3O_4_PEG-PLGA and FeHA were found to generate the TEMPONE radical, but not Fe_3O_4, TiHA and HA (Fig. 4A). The trend is in line with the oxidative potential inferred from the reactivity profiles (Fig. 2) and DTT depletion tests (Fig. 3). Note that TiHA is inert also under simulated solar irradiation, as previously reported.[35]

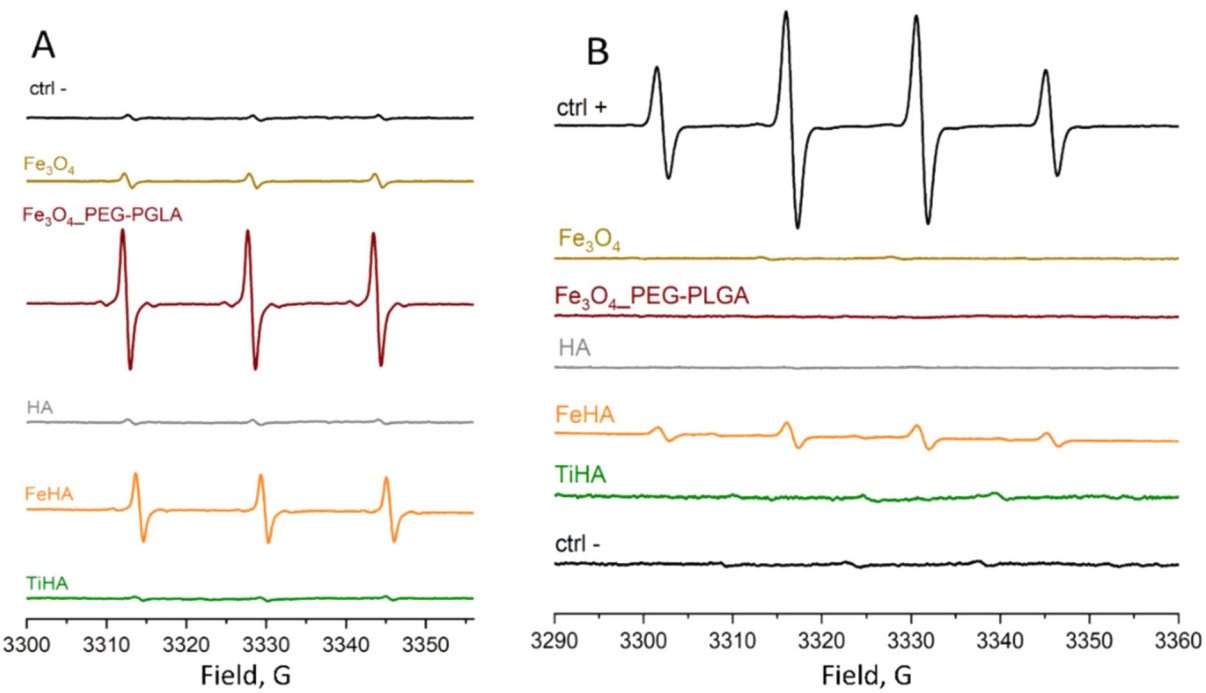

Fig. 4 EPR spectra. (A) Surface reactivity assessed using the TEMPONE-H probe molecule as a spin trap; (B) Fenton-like reactivity with the addition of hydrogen peroxide assessed using DMPO as a spin trap. Conditions: NBMs in phosphate buffer at pH 7.4.

This suggests that Ti ions are not photoreactive or are not in contact with the solvent since they are embedded in the HA matrix.

Due to the possible release of redox active ions, the experiments on Fe-based NBMs were repeated by testing the presence of free radicals in the supernatant obtained by centrifugation or filtration of the NBMs after incubation. Free radicals were found on the supernatant of FeHA, suggesting the role of dissolved iron ions, but not in the supernatant of Fe_3O_4_PEG-PLGA. This agrees with the dissolution experiments (Table S1†).

We investigated the formation of ROS also in the presence of H_2O_2. NBMs that are inert in water might still produce ROS in phagolysosomes once eventually phagocyted by immune system cells. In fact, in this cellular compartment, hydrogen peroxide is abundant and the presence of redox active metal ions (*e.g.*, Fe^{2+}) may catalyze the generation of hydroxyl radicals through Fenton-like[67,68] mechanisms:

$$H_2O_2 + e^- \rightarrow OH^- + OH^{\bullet}$$

Fig. 4B shows the EPR spectra of the NBMs in the presence of hydrogen peroxide. Among the samples, only FeHA showed the typical four-peak signal of hydroxyl radicals generated in the presence of the spin trap DMPO, but with intensity significantly lower that of the positive control, indicating the presence of redox-active iron, as confirmed by cyclic voltammetry measurements in PBS (Fig. 5).

Direct oxidation capacity. Redox active NBMs can react with biological molecules also by direct exchange of electrons, not mediated by radicals.[65] We investigated the extent of this mechanism, which adds to radical-mediated oxidation. Fe_3O_4 is the unique NBM in the series producing radicals, while FeHA induced the formation of ROS only in the presence of H_2O_2. Fig. 3, however, indicates that DTT is also consumed by the NBMs that do not generate ROS. Fig. 5 shows the cyclic voltammograms recorded for AgHEC, FeHA and Fe_3O_4_PEG-PLGA both in water and DMEM. The oxidation and reduction peaks of Ag-HEC (Fig. 5A) are eye-catching; the formation of a biocorona when the particles are exposed to DMEM does not quench the redox activity of the particles, which, evidently, are able to exchange electrons also in the presence of a layer of biological species at their surface. Some redox activity is also visible for Fe_3O_4-PEG-PLGA (Fig. 5B); a clear oxidation peak appears in water at around −0.2 V (black trace), while the relative reduction gives rise to a barely visible shoulder centered at −0.4 V. In DMEM (red trace), cyclic voltammetry exhibits only very low redox activity. Clearly, the redox behavior of this coated magnetite can be attributed only to the Fe ions at its

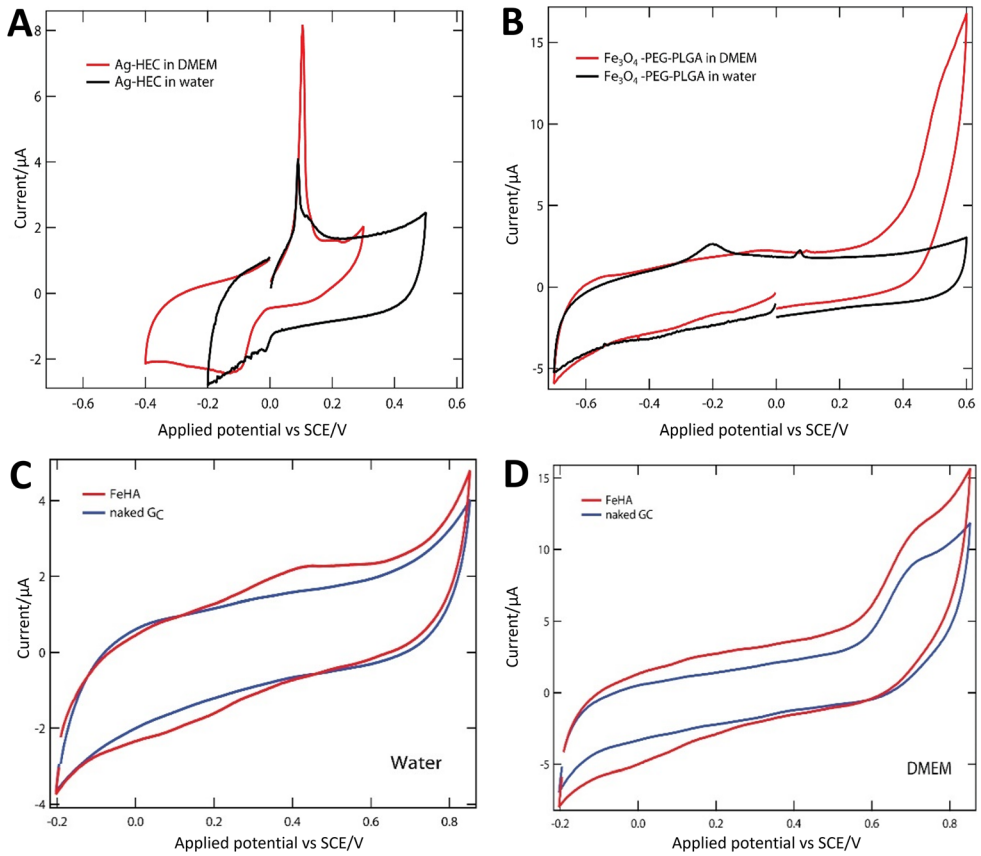

Fig. 5 Cyclic voltammograms of the NBMs deposited on a glassy carbon electrode. Top: (A) Ag-HEC and (B) Fe_3O_4_PEG-PLGA, both in water (black) and in DMEM medium (red). Bottom: FeHA in (C) water and (D) DMEM. Scan rate: 10 mV s^{-1}; supporting electrolyte: 10^{-2} M K_2SO_4.

surface. The presence of active Fe ions at the surface can also be hypothesized for the oxidizing activity of FeHA in DTT assay. For this doped hydroxyapatite, large, yet visible, oxidation and reduction bands were observed in water (red trace, Fig. 5C), while just a shoulder on the reduction potential region was observed in DMEM (red trace, Fig. 5D). All in all, these measurements revealed the possibility that the NBMs oxidize thiols also through direct interaction, which adds to the radical mediated oxidation.

Discussion

Fe and Ti doping alters the number and nature of surface reactive sites in HA-based NBMs

The late formation of formaldehyde and CO_2 in MeOH-TPSR for HA is indicative of redox and basic surface sites with low reactivity, compared to other metal oxides and multicomponent systems that under the same conditions over-oxidized methanol to CO_2 in their highly reactive redox sites, as inferred by relatively lower temperatures of CO_2 release (*e.g.*, 221 °C for CuO and 231 °C for $CuFe_2O_4$).[19] Importantly, the low reactivity exhibited by undoped HA confirmed its established biocompatibility, which justified its widespread use in medical applications.[51]

Metal doping in HA NBMs led to a decrease in the active site surface density from 5 to 2 active sites per nm^2 in both TiHA and FeHA. The surface area increase observed in the doped HA NBMs aligns with previous reports[69] and the trends seen in doped nano-oxides, where synthesis conditions and dopant incorporation promote smaller crystallites, enhanced porosity, and modified agglomeration.[70] In terms of surface reactivity, Fe doping shifted HA's reactivity towards more oxidative pathways; MeOH-TPSR tests revealed a slight redox activity, in line with FeHA's ability to oxidize DTT and TEMPONE-H, and to produce hydroxyl radicals by a Fenton-like reaction. Complementary CV data also revealed redox activity attributed to the presence of redox-active iron ions within the HA matrix. Consequently, the reactivity of FeHA involves two distinct mechanisms: surface-mediated heterogeneous reactivity and ion-mediated homogeneous reactions due to dopant release. The observed reactivity correlates with the reported ability of this material to induce intracellular ROS release in HCT116 cells, albeit no significant DNA damage was observed.[71]

Ti-doped HA maintained a low basic reactivity similar to that of HA, as seen by the CO_2 bands in MeOH-TPSR, but also exhibited acidic surface sites, as evidenced by the DME signal (Fig. 2E). In line with this, TiHA was poorly reactive toward DTT, in agreement with previous findings on similar TiO_2-HA nanomaterials.[19] The absence of reactivity under simulated solar irradiation further supports TiHA's inert behavior in the liquid phase, as Ti ions appear to be effectively embedded within the HA matrix, in line with previous studies in TiHA-based NBMs.[72] The low oxidative potential correlates with the absence of a notable increase in 53BP1 foci or micronucleus formation, as reported by Fontaine *et al.*[71] The enhanced acidic surface reactivity is not translated into significant adverse effects.[71]

Surface coatings regulate the oxidative reactivity of hybrid magnetite- and Ag-derived NBMs

Surface coatings transform the oxidative potential of NBMs. The reactivity of iron oxide nanoparticles has been extensively studied in the literature, and it has been related to oxidative stress, as observed in cells exposed to these materials.[73] The role of the iron redox state, however, has been found to be decisive for the toxicological effects; while Fe_2O_3 did not present any cytotoxic concentration up to 100 μg mL^{-1} for A549 cells,[11] superparamagnetic Fe_3O_4 nanoparticles induced cell DNA damage.[74] Additionally, the oxidative stress induced by Fe_3O_4 has been reported both by *in vivo*[75–78] and *in vitro*[79–82] studies. In previous works, a Fenton reaction mechanism involving iron ions was suggested as a hypothesis, where hydrogen peroxide interacts with Fe^{2+}, promoting its oxidation into Fe^{3+} and leading to localized oxidative stress, rather than diffusive ROS-mediated damage to cellular components such as DNA.[71] However, this topic has been a critical point of discussions. In a recent review, Muranov indicated that under physiological conditions iron transport is regulated by carrier proteins, minimizing the presence of free iron ions in the cytoplasm. However, in pathological states where the carrier protein function is impaired, iron ions may enter the cytosol. At near-neutral pH, typical of the cytosol, these ions form insoluble hydroxides, preventing the classical Fenton reaction. Nevertheless, these iron hydroxides can catalyze hydrogen peroxide decomposition, producing hydroxyl radicals in a Fenton-like reaction.[83] This reaction can be used for medical purposes, *e.g.*, in metal-based NBMs for tumor therapy.[84]

Distinct reactivity was observed for the uncoated and PEG-PLGA-coated Fe_3O_4 nanomaterials. Interestingly, DTT oxidation using Fe_3O_4_PEG-PLGA was comparable to that of highly reactive nanomaterials such as CuO[85,86] (positive control). This coated magnetite also showed significant salicylic acid hydroxylation, but did not produce detectable ROS. This pattern suggests that the oxidative properties of Fe_3O_4_PEG-PLGA are likely surface-based rather than mediated through ROS, highlighting the effect of the PEG-PLGA coating on Fe_3O_4's surface.[71] In line with our results, previous studies concluded that exposure of HCT116 cells to Fe_3O_4_PEG-PLGA led to a concentration-dependent increase of intracellular ROS content, but the absence of genotoxic effects.[71] Finally, Fe_3O_4 PEG-PLGA and Fe_3O_4 were tested *in vivo* in recent studies, showing no significant risks to the soil invertebrate model species *Enchytraeus crypticus* and *Folsomia candida*, as determined by the standard 28 day OECD test and an extended 56 day exposure version.[87]

In the case of the silver-based nanomaterials, uncoated Ag nanoparticles exhibited high intrinsic reactivity, as evidenced by substantial DTT depletion, aligning with previous studies on Ag's redox properties.[27] The reported gastrointestinal tox-

icity of uncoated silver nanoparticles was evaluated in human intestinal cells, producing significant cytotoxicity, increased ROS production, and DNA damage with only minor alterations in toxicity following simulated gastrointestinal digestion.[28] In AgHEC, the hydroxyethyl cellulose coating may stabilize Ag, modulating surface reactivity. This phenomenon is reflected in reduced toxicity, lower ROS generation, and less DNA damage than Ag, thanks to the protective coating that mitigated harmful interactions. Similarly, studies on the exposure of the alveolar epithelial cell line A549 to Ag and AgHEC reported significantly higher cytotoxicity, oxidative stress and cellular uptake by uncoated Ag nanoparticles, which led to greater ROS production.[88] Collectively, these observations underscore the role of oxidative stress as a driving mechanism of toxicity for Ag nanomaterials. The high oxidative potential of uncoated Ag, which correlates strongly with adverse biological outcomes, supports the hypothesis of a reactivity-triggered toxicity model for silver-based nanomaterials.[27]

In chemico approaches are required to deeply understand the complexity of hybrid nanobiomaterials

The oxidative potential of NBMs represents a critical factor in assessing their safety and applicability in biomedical contexts. While previously established methods, such as those detailed by Zhang *et al.* (2012), evaluated the oxidative potential of single-component materials (referred to as single metal nanooxides) through their well-defined electrochemical properties, these approaches often lack robustness when applied to hybrid NBMs.[89] Hybrid NBMs, by design, integrate multiple components to enhance stability, biocompatibility, or functionality, inherently complicating their surface reactivity profiles. This complexity necessitates the integration of *in chemico* methodologies to complement existing paradigms. Thus, our findings underscore that the surface reactivity, influenced by doping or coating strategies, is related to the nanomaterial composition, but cannot always be directly correlated with biological outcomes due to the involvement of additional factors such as cellular uptake and protein corona formation. However, in the frame of risk assessment, these *in chemico* reactive descriptors remain invaluable for identifying key initiating events in adverse outcome pathways (AOPs) and grouping approaches.[32,45,50] Furthermore, the concentration of reactive sites has been proposed as a refined dose metric in nanotoxicology[20] based on the premise that not only does the same mass not correspond to the same surface area, but also not all physical surface areas correspond to chemically active sites.[35] Consequently, when surface reactivity-driven toxicity is the primary adverse effect, this metric may provide a more accurate assessment of toxicological responses, rather than the mass, the traditional dose metric, or the surface area, as lately suggested.

Finally, the increasing focus on reducing animal testing has driven the development of NAMs, including *in silico* studies – computational methods designed to predict the toxicological behavior of nanomaterials.[90,91] These methods aim to identify toxicity patterns without requiring *in vivo* testing, relying instead on a few basic, easily measurable, and standardized properties, such as composition, structure, specific surface area, or reactivity.[92] However, these methods still suffer from a significant lack of datasets for proper training. Studies like ours, which generate extensive datasets, are particularly important for establishing correlations between physicochemical properties, variations in composition and nanomaterial characteristics, and their relationship with biocompatibility – mainly related to the interactions at the nano–bio interface.[93] Therefore, the *in chemico* NAM proposed has been described in detail in the ESI,† adding a series of steps to analyze new hybrid NBMs.

Conclusions and outlook

A methodology is presented that facilitates the development of safer NBMs, thereby enhancing their biocompatibility, by better understanding their differential surface and reactive properties. The *in chemico* strategy followed in this work leads to the conclusion that (1) doping of HA NBMs with Ti or Fe results in a more reactive surface with less active site surface density and, in the case of Fe doping, increased oxidative potential and (2) organic coatings modulate NBMs' reactivity, lowering the surface reactivity in the case of AgHEC, whereas the reactive-driven mechanism is modified in the case of Fe_3O_4_PEG-PLAG.

In terms of dose metrics, the determination of the number of surface sites and the description of the active site surface density aim to propose a refined dose for the assessment of NBMs. In line with our previous works, this approach focuses on evaluating the reactive surface sites of NBMs rather than relying exclusively on their mass or total surface area. By adopting this perspective, it has the potential to advance the field of nanotoxicology, enabling more precise and reliable risk/reactive assessments of new hybrid NBMs.

Data availability

The data supporting the findings of this study are available throughout the article and in the ESI.†

Conflicts of interest

There are no conflicts to declare.

Acknowledgements

The authors are grateful for the financial support from the European Commission through H2020 projects BioRiMa (GA760928) and NanoinformaTIX (GA814426).

References

1 W. Park, H. Shin, B. Choi, W. K. Rhim, K. Na and D. Keun Han, Advanced hybrid nanomaterials for biomedical applications, *Prog. Mater. Sci.*, 2020, **114**, 100686, DOI: 10.1016/J.PMATSCI.2020.100686.

2 I. Ul Haq and K. Krukiewicz, Antimicrobial approaches for medical implants coating to prevent implants associated infections: Insights to develop durable antimicrobial implants, *Appl. Surf. Sci. Adv.*, 2023, **18**, 100532, DOI: 10.1016/J.APSADV.2023.100532.

3 E. M. Materón, C. M. Miyazaki, O. Carr, *et al.*, Magnetic nanoparticles in biomedical applications: A review, *Appl. Surf. Sci. Adv.*, 2021, **6**, 100163, DOI: 10.1016/J.APSADV.2021.100163.

4 G. M. Manoj, M. Shalini, K. Thenmozhi, V. K. Ponnusamy and S. Hari, Recent advancements in the surface modification and functionalization of magnetic nanomaterials, *Appl. Surf. Sci. Adv.*, 2024, **21**, 100608, DOI: 10.1016/J.APSADV.2024.100608.

5 D. E. Radulescu, O. R. Vasile, E. Andronescu and A. Ficai, Latest Research of Doped Hydroxyapatite for Bone Tissue Engineering, *Int. J. Mol. Sci.*, 2023, **24**(17), 13157, DOI: 10.3390/IJMS241713157.

6 A. Cai, H. Yin, C. Wang, *et al.*, Photothermal effect and antibacterial properties of Zn2+, Cu2+ and Ag+ doped hydroxyapatite @ polydopamine on porous tantalum surface, *Appl. Surf. Sci.*, 2024, **649**, 159137, DOI: 10.1016/J.APSUSC.2023.159137.

7 A. S. Agnihotri, M. Nidhin, S. Rison, K. B. Akshaya and A. Varghese, Tuning of the surface structure of silver nanoparticles using Gum arabic for enhanced electrocatalytic oxidation of morin, *Appl. Surf. Sci. Adv.*, 2021, **6**, 100181, DOI: 10.1016/J.APSADV.2021.100181.

8 D. Bociaga, P. Komorowski, D. Batory, *et al.*, Silver-doped nanocomposite carbon coatings (Ag-DLC) for biomedical applications – Physiochemical and biological evaluation, *Appl. Surf. Sci.*, 2015, **355**, 388–397, DOI: 10.1016/J.APSUSC.2015.07.117.

9 H. R. Tantawy, A. A. Nada, A. Baraka and M. A. Elsayed, Novel synthesis of bimetallic Ag-Cu nanocatalysts for rapid oxidative and reductive degradation of anionic and cationic dyes, *Appl. Surf. Sci. Adv.*, 2021, **3**, 100056, DOI: 10.1016/J.APSADV.2021.100056.

10 N. B. Saleh, D. J. Milliron, N. Aich, L. E. Katz, H. M. Liljestrand and M. J. Kirisits, Importance of doping, dopant distribution, and defects on electronic band structure alteration of metal oxide nanoparticles: Implications for reactive oxygen species, *Sci. Total Environ.*, 2016, **568**, 926–932, DOI: 10.1016/J.SCITOTENV.2016.06.145.

11 V. Alcolea-Rodriguez, V. I. Dumit, R. Ledwith, R. Portela, M. A. Bañares and A. Haase, Differentially Induced Autophagy by Engineered Nanomaterial Treatment Has an Impact on Cellular Homeostasis and Cytotoxicity, *Nano Lett.*, 2024, **24**(38), 11793–11799, DOI: 10.1021/acs.nanolett.4c01573.

12 A. Bregnocchi, R. Jafari and G. Momen, Design strategies for antiviral coatings and surfaces: A review, *Appl. Surf. Sci. Adv.*, 2022, **8**, 100224, DOI: 10.1016/J.APSADV.2022.100224.

13 K. Saravanakumar, H. M. N. Iqbal and M. H. Wang, Nano-Surface Coatings-Inorganic and Organic Nano-Surface Coatings for Food Packaging and Dentistry, *Appl. Surf. Sci. Adv.*, 2024, **24**, 100653, DOI: 10.1016/J.APSADV.2024.100653.

14 D. Eleftheriadou, D. Kesidou, F. Moura, *et al.*, Redox-Responsive Nanobiomaterials-Based Therapeutics for Neurodegenerative Diseases, *Small*, 2020, **16**(43), 1907308, DOI: 10.1002/SMLL.201907308.

15 K. Gerloff, B. Landesmann, A. Worth, S. Munn, T. Palosaari and M. Whelan, The Adverse Outcome Pathway approach in nanotoxicology, *Comput. Toxicol.*, 2017, **1**, 3–11, DOI: 10.1016/j.comtox.2016.07.001.

16 J. Jeong and J. Choi, Use of adverse outcome pathways in chemical toxicity testing: potential advantages and limitations, *Environ. Health Toxicol.*, 2017, **33**(1), e2018002, DOI: 10.5620/eht.e2018002.

17 N. El Yamani, E. Mariussen, M. Gromelski, *et al.*, Hazard identification of nanomaterials: In silico unraveling of descriptors for cytotoxicity and genotoxicity, *Nano Today*, 2022, **46**, 101581, DOI: 10.1016/j.nantod.2022.101581.

18 M. T. D. Cronin, F. Bajot, S. J. Enoch, J. C. Madden, D. W. Roberts and J. Schwöbel, The in chemico-in silico interface: Challenges for integrating experimental and computational chemistry to identify toxicity, *ATLA, Altern. Lab. Anim.*, 2009, **37**(5), 513–521, DOI: 10.1177/026119290903700508.

19 V. Alcolea-Rodriguez, R. Portela, V. Calvino-Casilda and M. A. Bañares, *In chemico* methodology for engineered nanomaterial categorization according to number, nature and oxidative potential of reactive surface sites, *Environ. Sci. Nano.*, 2024, **11**(9), 3744–3760, DOI: 10.1039/D3EN00810J.

20 V. Alcolea-Rodriguez, N. Coca-López, F. Simeone, *et al.* A refined dose metrics for nanotoxicology based on surface sites reactivity for oxidative potential of engineered nanomaterials, *Nanoscale Adv.*, DOI: 10.1039/D5NA00104H, Published online 2025.

21 A. Kermanizadeh, S. Vranic, S. Boland, *et al.*, An in vitroassessment of panel of engineered nanomaterials using a human renal cell line: cytotoxicity, pro-inflammatory response, oxidative stress and genotoxicity, *BMC Nephrol.*, 2013, **14**(1), 96, DOI: 10.1186/1471-2369-14-96.

22 C. F. Jones and D. W. Grainger, In vitro assessments of nanomaterial toxicity, *Adv. Drug Delivery Rev.*, 2009, **61**(6), 438–456, DOI: 10.1016/j.addr.2009.03.005.

23 A. Solorio-Rodríguez, V. Escamilla-Rivera, M. Uribe-Ramírez, *et al.*, In vitro cytotoxicity study of superparamagnetic iron oxide and silica nanoparticles on pneumocyte organelles, *Toxicol. in Vitro*, 2021, **72**, 105071, DOI: 10.1016/j.tiv.2020.105071.

24 W. Lin, Y. W. Huang, X. D. Zhou and Y. Ma, In vitro toxicity of silica nanoparticles in human lung cancer cells, *Toxicol.*

Appl. Pharmacol., 2006, **217**(3), 252–259, DOI: 10.1016/j.taap.2006.10.004.

25 T. Stobernack, N. Dommershausen, V. Alcolea-Rodríguez, *et al.*, Advancing Nanomaterial Toxicology Screening Through Efficient and Cost–Effective Quantitative Proteomics, *Small Methods*, 2024, **8**(12), 2400420, DOI: 10.1002/smtd.202400420.

26 G. Motta, M. Gualtieri, R. Bengalli, *et al.*, An integrated new approach methodology for inhalation risk assessment of safe and sustainable by design nanomaterials, *Environ. Int.*, 2024, **183**, 108420, DOI: 10.1016/J.ENVINT.2024.108420.

27 O. Kose, P. Mantecca, A. Costa and M. Carrière, Putative adverse outcome pathways for silver nanoparticle toxicity on mammalian male reproductive system: a literature review, *Part. Fibre Toxicol.*, 2023, **20**(1), 1–23, DOI: 10.1186/S12989-022-00511-9.

28 O. Kose, D. Béal, S. Motellier, *et al.*, Physicochemical Transformations of Silver Nanoparticles in the Oro-Gastrointestinal Tract Mildly Affect Their Toxicity to Intestinal Cells In Vitro: An AOP-Oriented Testing Approach, *Toxics*, 2023, **11**(3), 199, DOI: 10.3390/TOXICS11030199/S1.

29 S. Schmeisser, A. Miccoli, M. von Bergen, *et al.*, New approach methodologies in human regulatory toxicology – Not if, but how and when!, *Environ. Int.*, 2023, **178**, 108082, DOI: 10.1016/j.envint.2023.108082.

30 S. H. Doak, M. J. D. Clift, A. Costa, *et al.* The Road to Achieving the European Commission's Chemicals Strategy for Nanomaterial Sustainability—A PATROLS Perspective on New Approach Methodologies, *Small*, 2022, **18**(17), 2200231, DOI: 10.1002/smll.202200231.

31 G. Antonello, A. Marucco, E. Gazzano, *et al.*, Changes of physico-chemical properties of nano-biomaterials by digestion fluids affect the physiological properties of epithelial intestinal cells and barrier models, *Part. Fibre Toxicol.*, 2022, **19**(1), 1–28, DOI: 10.1186/S12989-022-00491-W.

32 S. I. L. Gomes, I. Zanoni, M. Blosi, *et al.*, Safe and sustainable by design Ag nanomaterials: A case study to evaluate the bio-reactivity in the environment using a soil model invertebrate, *Sci. Total Environ.*, 2024, **927**, 171860, DOI: 10.1016/J.SCITOTENV.2024.171860.

33 D. Hernández-Moreno, J. M. Navas and M. L. Fernández-Cruz, Short and long-term effects of nanobiomaterials in fish cell lines. Applicability of RTgill-W1, *Chemosphere*, 2022, **309**, 136636, DOI: 10.1016/j.chemosphere.2022.136636.

34 S. Martin, L. de Haan, I. Miro Estruch, *et al.*, Pre-validation of a reporter gene assay for oxidative stress for the rapid screening of nanobiomaterials, *Front. Toxicol.*, 2022, **4**, 974429, DOI: 10.3389/FTOX.2022.974429/BIBTEX.

35 M. A. Bañares, V. Alcolea-Rodriguez and R. Portela, A catalytic perspective to nanomaterials reactivity-based toxicity; implications for single- and multiple-component nanomaterials (nanocomposites), *NanoImpact*, 2025, **37**, 100542, DOI: 10.1016/J.IMPACT.2025.100542.

36 L. Armand, M. Biola-Clier, L. Bobyk, *et al.* Molecular responses of alveolar epithelial A549 cells to chronic exposure to titanium dioxide nanoparticles: A proteomic view, *J. Proteomics.*, 2016, **134**, 163–173, DOI: 10.1016/j.jprot.2015.08.006.

37 M. Dusinska, E. Rundén-Pran, J. Schnekenburger and J. Kanno, Toxicity Tests: In Vitro and In Vivo, in *Adverse Effects of Engineered Nanomaterials*, Elsevier, 2nd edn, 2017, pp. 51–82. DOI: 10.1016/B978-0-12-809199-9.00003-3.

38 A. Bannuscher, B. Hellack, A. Bahl, *et al.*, Metabolomics profiling to investigate nanomaterial toxicity in vitro and in vivo, *Nanotoxicology*, 2020, **14**(6), 807–826, DOI: 10.1080/17435390.2020.1764123.

39 B. Trouiller, R. Reliene, P. Solaimani and R. H. Schiestl, Titanium dioxide nanoparticles induce DNA damage and genetic instability in vivo in mice, *Cancer Res.*, 2009, **69**(22), 8784–8789, DOI: 10.1158/0008-5472.CAN-09-2496.

40 K. D. Patel, Z. Keskin-Erdogan, P. Sawadkar, *et al.*, Oxidative stress modulating nanomaterials and their biochemical roles in nanomedicine, *Nanoscale Horiz.*, 2024, **9**(10), 1630–1682, DOI: 10.1039/D4NH00171K.

41 Y. Luo and Y. Wu, Defect Engineering of Nanomaterials for Catalysis, *Nanomaterials*, 2023, **13**(6), 1116, DOI: 10.3390/NANO13061116.

42 F. M. Pinto, V. Y. Suzuki, R. C. Silva and F. A. La Porta, Oxygen Defects and Surface Chemistry of Reducible Oxides, *Front. Mater.*, 2019, **6**, 466671, DOI: 10.3389/FMATS.2019.00260/BIBTEX.

43 S. T. Kim, K. Saha, C. Kim and V. M. Rotello, The role of surface functionality in determining nanoparticle cytotoxicity, *Acc. Chem. Res.*, 2013, **46**(3), 681–691, DOI: 10.1021/AR3000647/ASSET/IMAGES/LARGE/AR-2012-000647_0010.JPEG.

44 A. Serrano-Lotina, R. Portela, P. Baeza, V. Alcolea-Rodriguez, M. Villarroel and P. Ávila, Zeta potential as a tool for functional materials development, *Catal. Today*, 2023, **423**, 113862, DOI: 10.1016/j.cattod.2022.08.004.

45 D. Ag Seleci, G. Tsiliki, K. Werle, *et al.*, Determining nanoform similarity via assessment of surface reactivity by abiotic and in vitro assays, *NanoImpact*, 2022, **26**, 100390, DOI: 10.1016/j.impact.2022.100390.

46 H. Choi, B. Choi, J. Han, H. E. Shin, W. Park and D. Kim, Reactive Oxygen Species Responsive Cleavable Hierarchical Metallic Supra–Nanostructure, *Small*, 2022, **18**(38), 2202694, DOI: 10.1002/smll.202202694.

47 A. Manke, L. Wang and Y. Rojanasakul, Mechanisms of Nanoparticle-Induced Oxidative Stress and Toxicity, *Biomed. Res. Int.*, 2013, **2013**, 1–15, DOI: 10.1155/2013/942916.

48 N. Jeliazkova, E. Bleeker, R. Cross, *et al.*, How can we justify grouping of nanoforms for hazard assessment? Concepts and tools to quantify similarity, *NanoImpact*, 2022, **25**, 100366, DOI: 10.1016/j.impact.2021.100366.

49 V. Stone, S. Gottardo, E. A. J. Bleeker, *et al.*, A framework for grouping and read-across of nanomaterials- supporting innovation and risk assessment, *Nano Today*, 2020, **35**, 100941, DOI: 10.1016/j.nantod.2020.100941.

50 A. Bahl, B. Hellack, M. Wiemann, *et al.*, Nanomaterial categorization by surface reactivity: A case study comparing 35 materials with four different test methods, *NanoImpact*, 2020, **19**, 100234, DOI: 10.1016/j.impact.2020.100234.
51 S. I. L. Gomes, B. Guimarães, E. Campodoni, *et al.*, Safer and Sustainable-by-Design Hydroxyapatite Nanobiomaterials for Biomedical Applications: Assessment of Environmental Hazards, *Nanomaterials*, 2022, **12**(22), 4060, DOI: 10.3390/NANO12224060/S1.
52 A. L. Costa, M. Blosi, A. Brigliadori, *et al.*, Eco design for Ag-based solutions against SARS-CoV-2 and *E. coli*, *Environ. Sci. Nano.*, 2022, **9**(11), 4295–4304, DOI: 10.1039/D2EN00178K.
53 M. Blosi, A. Brigliadori, S. Ortelli, *et al.*, Re-designing nano-silver technology exploiting one-pot hydroxyethyl cellulose-driven green synthesis, *Front. Chem.*, 2024, **12**, 1432546, DOI: 10.3389/FCHEM.2024.1432546/BIBTEX.
54 M. Fontaine, E. Bartolami, M. Prono, *et al.*, Nanomaterial genotoxicity evaluation using the high-throughput p53-binding protein 1 (53BP1) assay, *PLoS One*, 2023, **18**, 1–29, DOI: 10.1371/journal.pone.0288737.
55 S. I. L. Gomes, B. Guimarães, E. Campodoni, *et al.*, Safer and Sustainable-by-Design Hydroxyapatite Nanobiomaterials for Biomedical Applications: Assessment of Environmental Hazards, *Nanomaterials*, 2023, **18**(9), e0288737, DOI: 10.3390/nano12224060.
56 K. A. Jensen, NanoGenoTox. WP4, Deliverable 3: Final Protocol for Producing Suitable MN Exposure Media. The Generic NANOGENOTOX Dispersion Protocol. Standard Operation Procedure (SOP) and Background Documentation, 2011.
57 M. J. Burgum, V. Alcolea-Rodríguez, H. Saarelainen, *et al.*, The dispersion method does not affect the in vitro genotoxicity of multi-walled carbon nanotubes despite inducing surface alterations, *NanoImpact*, 2025, **37**, 100539, DOI: 10.1016/J.IMPACT.2024.100539.
58 H. Jiang, C. M. Sabbir Ahmed, A. Canchola, J. Y. Chen and Y. H. Lin, Use of dithiothreitol assay to evaluate the oxidative potential of atmospheric aerosols, *Atmosphere*, 2019, **10**(10), 1–21, DOI: 10.3390/atmos10100571.
59 B. Halliwell, M. Grootveld and J. M. C. Gutteridge, Methods for the Measurement of Hydroxyl Radicals in Biochemical Systems: Deoxyribose Degradation and Aromatic Hydroxylation, *Methods Biochem. Anal.*, 2006, **33**, 59–90, DOI: 10.1002/9780470110546.CH2.
60 A. Ghiselli, O. Laurenti, G. De Mattia, G. Maiani and A. Ferro-Luzzi, Salicylate hydroxylation as an early marker of in vivo oxidative stress in diabetic patients, *Free Radical Biol. Med.*, 1992, **13**(6), 621–626, DOI: 10.1016/0891-5849(92)90036-G.
61 S. Ortelli, M. Blosi, C. Delpivo, *et al.*, Multiple approach to test nano TiO2 photo-activity, *J. Photochem. Photobiol., A*, 2014, **292**, 26–33, DOI: 10.1016/J.JPHOTOCHEM.2014.07.006.
62 K. Tschulik, C. Batchelor-Mcauley, H. S. Toh, E. J. E. Stuart and R. G. Compton, Electrochemical studies of silver nanoparticles: a guide for experimentalists and a perspective, *Phys. Chem. Chem. Phys.*, 2013, **16**(2), 616–623, DOI: 10.1039/C3CP54221A.
63 A. L. Kramer, S. Dorn, A. Perez, *et al.*, Assessing the oxidative potential of PAHs in ambient PM2.5 using the DTT consumption assay, *Environ. Pollut.*, 2021, **285**, 117411, DOI: 10.1016/j.envpol.2021.117411.
64 J. J. Sauvain, S. Deslarzes and M. Riediker, Nanoparticle reactivity toward dithiothreitol, *Nanotoxicology*, 2008, **2**(3), 121–129, DOI: 10.1080/17435390802245716.
65 J. G. Charrier and C. Anastasio, On dithiothreitol (DTT) as a measure of oxidative potential for ambient particles: evidence for the importance of soluble transition metals, *Atmos. Chem. Phys.*, 2012, **12**(19), 9321–9333, DOI: 10.5194/acp-12-9321-2012.
66 K. Ulrich and U. Jakob, The role of thiols in antioxidant systems, *Free Radical Biol. Med.*, 2019, **140**, 14–27, DOI: 10.1016/J.FREERADBIOMED.2019.05.035.
67 N. Zhang, G. Zhang, T. Huang, S. Chong and Y. Liu, Fe3O4 and Fe3O4/Fe2+/Fe0 catalyzed Fenton-like process for advanced treatment of pharmaceutical wastewater, *Desalin. Water Treat.*, 2017, **93**, 100–108, DOI: 10.5004/dwt.2017.21453.
68 E. G. Heckert, S. Seal and W. T. Self, Fenton-like reaction catalyzed by the rare earth inner transition metal cerium, *Environ. Sci. Technol.*, 2008, **42**(13), 5014–5019, DOI: 10.1021/ES8001508.
69 Z. Chen, Y. Liu, L. Mao, L. Gong, W. Sun and L. Feng, Effect of cation doping on the structure of hydroxyapatite and the mechanism of defluoridation, *Ceram. Int.*, 2018, **44**(6), 6002–6009, DOI: 10.1016/J.CERAMINT.2017.12.191.
70 E. W. McFarland and H. Metiu, Catalysis by doped oxides, *Chem. Rev.*, 2013, **113**(6), 4391–4427, DOI: 10.1021/CR300418S/ASSET/IMAGES/MEDIUM/CR-2012-00418S_0013.GIF.
71 M. Fontaine, E. Bartolami, M. Prono, *et al.*, Nanomaterial genotoxicity evaluation using the high-throughput p53-binding protein 1 (53BP1) assay, *PLoS One*, 2023, **18**, 1–29, DOI: 10.1371/journal.pone.0288737.
72 E. Campodoni, M. Montanari, C. Artusi, *et al.*, Biomineralization: A new tool for developing eco-sustainable Ti-doped hydroxyapatite-based hybrid UV filters, *Biomater. Adv.*, 2023, **151**, 213474, DOI: 10.1016/J.BIOADV.2023.213474.
73 S. Vercellino, I. Kokalari, M. Liz Cantoral, *et al.*, Biological interactions of ferromagnetic iron oxide–carbon nanohybrids with alveolar epithelial cells, *Biomater. Sci.*, 2022, **10**(13), 3514–3526, DOI: 10.1039/D2BM00220E.
74 N. Singh, G. J. S. Jenkins, B. C. Nelson, *et al.*, The role of iron redox state in the genotoxicity of ultrafine superparamagnetic iron oxide nanoparticles, *Biomaterials*, 2012, **33**(1), 163–170, DOI: 10.1016/J.BIOMATERIALS.2011.09.087.
75 W. Zhang, J. Gao, L. Lu, *et al.*, Intracellular GSH/GST antioxidants system change as an earlier biomarker for toxicity evaluation of iron oxide nanoparticles, *NanoImpact*, 2021, **23**, 100338, DOI: 10.1016/J.IMPACT.2021.100338.
76 L. Wu, W. Wen, X. Wang, *et al.*, Ultrasmall iron oxide nanoparticles cause significant toxicity by specifically inducing

acute oxidative stress to multiple organs, *Part. Fibre Toxicol.*, 2022, **19**(1), 1–14, DOI: **10.1186/S12989-022-00465-Y/FIGURES/7**.

77 K. Volkovova, R. D. Handy, M. Staruchova, *et al.*, Health effects of selected nanoparticles in vivo: liver function and hepatotoxicity following intravenous injection of titanium dioxide and Na-oleate-coated iron oxide nanoparticles in rodents, *Nanotoxicology*, 2015, **9**(S1), 95–105, DOI: **10.3109/17435390.2013.815285**.

78 Y. Baratli, A. L. Charles, V. Wolff, *et al.*, Age Modulates Fe3O4 Nanoparticles Liver Toxicity: Dose-Dependent Decrease in Mitochondrial Respiratory Chain Complexes Activities and Coupling in Middle-Aged as Compared to Young Rats, *Biomed. Res. Int.*, 2014, **2014**(1), 474081, DOI: **10.1155/2014/474081**.

79 Y. Xie, D. Liu, C. Cai, *et al.*, Size-dependent cytotoxicity of Fe3O4 nanoparticles induced by biphasic regulation of oxidative stress in different human hepatoma cells, *Int. J. Nanomed.*, 2016, **11**, 3557–3570, DOI: **10.2147/IJN.S105575**.

80 A. G. Ranjbary, G. K. Saleh, M. Azimi, F. Karimian, J. Mehrzad and J. Zohdi, Superparamagnetic Iron Oxide Nanoparticles Induce Apoptosis in HT-29 Cells by Stimulating Oxidative Stress and Damaging DNA, *Biol. Trace Elem. Res.*, 2023, **201**(3), 1163–1173, DOI: **10.1007/S12011-022-03229-Z/FIGURES/4**.

81 J. Duan, V. K. Kodali, M. J. Gaffrey, *et al.*, Quantitative profiling of protein s-glutathionylation reveals redox-dependent regulation of macrophage function during nanoparticle-induced oxidative stress, *ACS Nano*, 2016, **10**(1), 524–538, DOI: **10.1021/ACSNANO.5B05524/ASSET/IMAGES/LARGE/NN-2015-05524N_0009.JPEG**.

82 J. A. Adeyemi, C. A. Sorgi, A. R. T. Machado, *et al.*, Phospholipids modifications in human hepatoma cell lines (HepG2) exposed to silver and iron oxide nanoparticles, *Arch. Toxicol.*, 2020, **94**(8), 2625–2636, DOI: **10.1007/S00204-020-02789-0/FIGURES/7**.

83 K. O. Muranov, Fenton Reaction in vivo and in vitro. Possibilities and Limitations, *Biochemistry (Moscow)*, 2024, **89**(1), S112–S126, DOI: **10.1134/S0006297924140074**.

84 W. Cao, M. Jin, K. Yang, *et al.*, Fenton/Fenton-like metal-based nanomaterials combine with oxidase for synergistic tumor therapy, *J. Nanobiotechnol.*, 2021, **19**, 325, DOI: **10.1186/S12951-021-01074-1**.

85 E. Moschini, G. Colombo, G. Chirico, G. Capitani, I. Dalle-Donne and P. Mantecca, *Sci. Rep.*, 2023, **13**, 2326, DOI: **10.1038/s41598-023-28958-6**.

86 J. T. Kwon, Y. Kim, S. Choi, *et al.*, Pulmonary Toxicity and Proteomic Analysis in Bronchoalveolar Lavage Fluids and Lungs of Rats Exposed to Copper Oxide Nanoparticles, *Int. J. Mol. Sci.*, 2022, **23**(21), 13265, DOI: **10.3390/ijms232113265**.

87 S. I. L. Gomes, J. J. Scott-Fordsmand and M. J. B. Amorim, Iron Oxide (Magnetite)-Based Nanobiomaterial with Medical Applications—Environmental Hazard Assessment Using Terrestrial Model Species, *J. Xenobiot.*, 2024, **14**(1), 285–294, DOI: **10.3390/JOX14010017/S1**.

88 G. Motta, M. Gualtieri, M. Saibene, *et al.* Preliminary Toxicological Analysis in a Safe-by-Design and Adverse Outcome Pathway-Driven Approach on Different Silver Nanoparticles: Assessment of Acute Responses in A549 Cells, *Toxics*, 2023, **11**(2), 195, DOI: **10.3390/toxics11020195**.

89 H. Zhang, Z. Ji, T. Xia, *et al.*, Use of Metal Oxide Nanoparticle Band Gap To Develop a Predictive Paradigm for Oxidative Stress and Acute Pulmonary Inflammation, *ACS Nano*, 2012, **6**(5), 4349–4368, DOI: **10.1021/nn3010087**.

90 B. Fadeel, L. Farcal, B. Hardy, *et al.*, Advanced tools for the safety assessment of nanomaterials, *Nat. Nanotechnol.*, 2018, **13**(7), 537–543, DOI: **10.1038/s41565-018-0185-0**.

91 N. L. von Ranke, R. B. Geraldo, A. Lima dos Santos, *et al.*, Applying in silico approaches to nanotoxicology: Current status and future potential, *Comput. Toxicol.*, 2022, **22**, 100225, DOI: **10.1016/j.comtox.2022.100225**.

92 T. Puzyn, B. Rasulev, A. Gajewicz, *et al.*, Using nano-QSAR to predict the cytotoxicity of metal oxide nanoparticles, *Nat. Nanotechnol.*, 2011, **6**(3), 175–178, DOI: **10.1038/nnano.2011.10**.

93 A. E. Nel, L. Mädler, D. Velegol, *et al.*, Understanding biophysicochemical interactions at the nano–bio interface, *Nat. Mater.*, 2009, **8**(7), 543–557, DOI: **10.1038/nmat2442**.